ATMOSPHERIC SCIENCE LETTERS
Atmos. Sci. Let. **17**: 169–176 (2016)
Published online 15 December 2015 in Wiley Online Library
(wileyonlinelibrary.com) **DOI:** 10.1002/asl.639

RMetS
Royal Meteorological Society

Phase-locked tropical Pacific precipitation

Scott Curtis[1]* and David H. Douglass[2]

[1]*Department of Geography, Planning, and Environment, East Carolina University, Greenville, NC, USA*
[2]*Department of Physics and Astronomy, University of Rochester, NY, USA*

**Correspondence to:*
S. Curtis, Department of Geography, Planning, and Environment, East Carolina University, Brewster A232, Greenville, NC 27858, USA.
E-mail: curtisw@ecu.edu

Received: 9 June 2015
Revised: 27 October 2015
Accepted: 29 October 2015

Abstract

Prior studies of the El Niño/La Niña index *SST3.4* showed periodicity of exactly 2 or 3 years which were 'phase-locked' to the annual solar cycle. Ten such phase-locked intervals since 1870 were found. This article extends this work by studying precipitation data (*P34*) for the same region. We find phase-locked segments corresponding to those found in *SST3.4*. Each segment agrees both in the period of oscillation and the date interval. However, the temperature-precipitation relationship changes from segment to segment, demonstrating the non-stationarity of the system. The beginnings and ends of these time segments agree with previously reported abrupt climate shifts.

Keywords: **precipitation; El Nino; phase lock; SST; Nino 3.4**

1. Introduction

Many of the indices of the Earth's atmosphere–ocean climate system show rapid changes in a short time interval. These are called climate shifts. One of the most studied of these climate shifts is the 'Pacific climate shift' in the mid-1970s (Trenberth, 1990; Ebbesmeyer *et al.*, 1991; Bratcher and Giese, 2002). For example, the temperature of the Pacific Ocean increased by a large fraction of a degree during the mid-1970s. Abrupt climate shifts in a set of four climate indices (El Niño/La Niña index SST3.4, north and south Pacific indices, and the Atlantic multidecadal oscillation AMO) were reported by Douglass (2010). He found 18 such events since 1870 including the 'climate shift of the mid-1970s'. The importance of these observations is that if a climate index undergoes an abrupt climate shift the assumption of continuity in time of that index is questionable.

The relationship of climate shifts and phase-locked states was studied by Douglass (2011) in a detailed study of the El Niño/La Niña index SST3.4 from 1870 to 2010. He reported ten distinct time segments having period of oscillation of exactly 2 or 3 years. In his study the beginning and/or end dates of these phase-locked time segments had a near one-to-one correspondence with the previously reported climate shifts. In a later study four more climate indices all showed the phase-locked phenomena (Douglass, 2013).

What is phase locking? Phase locking occurs when a signal of frequency f_1 from a system has a fixed phase with respect to that of a second signal from the same system of frequency $f_2 = (n/m)\, f_1$, where n and m are integers. The relationship is usually a result of a non-linear mechanism within that system. A familiar example of phase-locking phenomena is that of a child 'pumping' on a swing to sustain the oscillating motion. The oscillation frequency is at the second subharmonic of the 'pump' frequency.

In a later article Douglass and Knox (2015a) (henceforth DK1) have confirmed that the central equatorial Pacific sea surface temperature index *SST3.4* has segments whose period of oscillation are a multiple of one year and were phase locked to an annual forcing of solar origin. DK1 extended the study of Douglass (2011) who identified ten 2- or 3-year phase-locked segments in *aSST3.4* in the time interval 1870–2008 and also referenced prior studies of geophysical indices (G) that also exhibited the same phase-locked behavior. These other geophysical indices were: (1) *SOI*, atmospheric pressure variation in the western Pacific; (2) *TLT*, temperature anomalies in the tropical troposphere; and (3) *W3*, tropical easterly winds. Also, phase locking is observed in the global ocean (Douglass and Knox, 2015b).

For all these indices, G, it is asserted that the climate system is being driven by a forcing $\boldsymbol{F}$ at a frequency of 1.0 cycles year^{-1} of Solar origin that causes two signals to be generated. The first, hG, is a direct response at 1.0 cycles year^{-1}. The second, aG, is a low frequency signal ($<$1.0 cycles year^{-1}) that represents the El Niño/La Niña phenomena. It is observed that the low frequency signal aG may contain time segments phase-locked at the second and third subharmonic of 1.0 cycles year^{-1}–i.e. at periods of 2 and 3 years. It is presumed that the subharmonics are generated though a nonlinear interaction in the climate system. This article studies the precipitation (P) response.

The development of global satellite-based precipitation data sets has facilitated the study of surface temperature–precipitation relationships at a variety of time scales. The Global Precipitation Climatology Project (GPCP) monthly product was commissioned by the World Climate Research Program to provide a long-term climatology of precipitation (Adler *et al.*, 2003). The objective of GPCP is to merge the

best available satellite data, taking advantage of the strengths of each source.

A number of recent papers have used GPCP to relate precipitation to surface temperatures (Adler *et al.*, 2008; Allan *et al.*, 2010; Gu and Adler, 2011; Liu and Allan, 2012). All these studies show a positive correlation between precipitation and temperature over tropical oceans (30°S to 30°N) and a negative correlation over land driven by the El Niño/La Niña phenomenon. According to the principle of thermodynamics, a warm ocean surface would increase humidity, cloudiness, and precipitation, whereas a warm land surface is indicative of sinking air and decreased humidity, cloudiness, and precipitation. During El Niño, precipitation increases over the central to eastern Pacific Ocean due to the ocean surface warming, and decreases over the Maritime Continent and equatorial South America and Africa due to anomalous subsidence caused by a shift in the Walker Circulation. Finally, Gu and Adler (2011) note that the strongest positive correlation between GPCP averaged over the tropical oceans and Nino *3.4 SST* anomalies is when the precipitation lags by about 2 months.

In Section 2 the source of the data is given. In Section 3 the methods are described. In Section 4 the data are analyzed. Discussion and results are given in Section 5.

2. Data

The precipitation (*P*) and surface sea temperature (*SST*) studied in this article are from Region3.4 in the tropical equatorial Pacific (latitude 5°S to 5°N and longitude 120 to 170°W). The precipitation data *P* comes from GPCP version 2.2 (Huffman *et al.*, 2009; NASA/GSFC, 2015). The values of *P* averaged over Region3.4 are named *P34*. The data are monthly from January 1979 to May 2014. The units are mm day^{-1}. The sea surface temperature (*SST*) data set, *SST3.4*, are found at (NOAA/CPC, 2015). The average of *SST* over Region3.4 is named *SST3.4* and is commonly used to study the El Niño/La Niña phenomenon.

3. Methods

The methods are described in DK1 and are summarized in this section.

3.1. Precise separation of high- and low-frequency effects

Studies of many geophysical phenomena start with a parent signal G_0, such as a temperature, wind speed or precipitation record, containing a component of interest mixed in with a seasonal component at frequencies of 1.0 cycle year^{-1} and its harmonics. The component of interest might show El Niño/La Niña effects with multi-year periodicity. An important task is to separate the annual component from G_0 to obtain the one of interest. A moving average filter is used to make this separation. Such a filter of length one year, which we denote by an operator $\boldsymbol{F}$, is the most effective. DK1 in their study of the El Niño/La Niña phenomena showed that the seasonal signal should be considered an essential component of the phenomena and be retained for study.

In the analysis only anomalies from the mean are treated. Thus we replace a parent series G_0 by $G = G_0 - \langle G_0 \rangle$, where $\langle G_0 \rangle$ is the average of the parent series over the range of the data.

The filter $\boldsymbol{F}$ is applied to the series G to create a 'season-free' anomaly aG defined as

$$aG = \mathbf{F}\,(\mathrm{G})\,. \tag{1}$$

This low frequency signal may contain the familiar El Niño/La Niña phenomena. A 'high frequency' index is also defined by

$$hG = G - \mathbf{F}\,(\mathrm{G}) \tag{2}$$

Both *SST3.4* and *P34* are 'parent' data. Thus, hG and aG can be calculated.

Note that the low frequency index given by Equation (1) poses a direct challenge to the commonly used climatology method of removing the seasonal effect. The climatology method for the case of monthly data consists of creating a climatology function $\boldsymbol{C}$ of frequency 1.0 cycle year^{-1} whose 12 monthly values are an average for each month over G for a particular time interval. The climate anomaly by this method is constructed by subtracting the climatology function from the values of G. Douglass (2011) has shown in detail that the climatology method can never completely remove the annual signal while the $\boldsymbol{F}$-filter method does.

3.2. Identifying phase-locked time segments

The sections above state that abrupt climate shifts in a geophysical index aG are associated with the beginning and or the ends of a segment of a geophysical time series showing oscillations of an exact multiple of one year. One way of identifying these segments is to examine the autocorrelation function versus delay time τ of a candidate segment. If the segment contains a component whose period is a multiple of one year then the autocorrelation function *vs* delay τ will be a cosine-like function with a minimum at $\tau/2$ and a maximum at τ; the value of τ will be a multiple of one year. The location and extent of such a segment in time are determined by adding or subtracting beginning- and end-date data points from a candidate segment until a cosine-like pattern appears.

4. Analysis

Figure 1(a) displays the original (parent) precipitation *P34* data showing an average of 2.12 mm day^{-1} and a

trend of −0.0296 (mm day^{-1}) year^{-1}. Also shown are the filtered precipitation data, $\boldsymbol{F}(P34)$. Figure 1(b) shows precipitation *aP34* as well as the sea surface temperature index, *aSST3.4*.

4.1. Precipitation index *hP34*

Because precipitation *P34* is a 'parent' data set one is able to calculate precipitation index *hP34*. Figure 2(a) shows precipitation index *hP34*, the high frequency component of precipitation *P34*. The autocorrelation function applied to precipitation index *hP34* in Figure 2(b) clearly shows sustained oscillations at 1.0 cycles year^{-1} as was found for sea surface temperature index *SST3.4* in DKI. The phase of the annual cycle is shown in Figure 2(c) where the average precipitation index *hP34* for each of the 12 months is plotted. The maximum occurs in April.

4.2. Phase-locked states of precipitation index *aP34*.

Figure 1(b) shows precipitation index *aP34* and sea surface temperature index *aSST3.4*. Four phase-locked segments of precipitation index *aP34* were found by the autocorrelation method described in Section 3.2. The date ranges were nearly identical to those found for sea surface temperature index *aSST3.4* and are indicated by shaded rectangles. The numbering, range and phase-locking periodicities are nearly the same as in Douglass (2011) (See Table 1).

The autocorrelation plots of these four segments are shown in Figure 3(a). These plots clearly show that segments 8, 9 and 11 have a periodicity of 3 years while segment 10 has periodicity of 2 years.

Phase-locking was demonstrated for these four segments for sea surface temperature index *aSST3.4* (DK1) by constructing a Lissajous plot. (Note. A Lissajous plot is a plot of two periodic signals vs each other where their frequency ratio is a rational fraction. The resulting plot is closed. One useful introduction is in Weisstein (2015). For the case in which the ratio is 2 to 1 the closed curve has two loops. We do the same for precipitation index *aP34* for segments 9 and 10. The average temperature for each month during a phase-locked segment was computed. For segment 9 (1990–2000) there were about three oscillations of period 3 years. So each of the 36 months had about three values in the average. This is shown in Figure 3(b), where the maximum in November corresponds to the years 1991, 1994 and 1997; this is the same result that was found for sea surface temperature index *aSST3.4*. (Note: the maximum at November 1997 is better known as the El Niño of 1997, the largest such event in a century.) The same calculations for the 2-year segment 10 (2002–2008) is shown in Figure 3(c). Note that this is a low amplitude manifestation (Figure 1(b)), and the y-axis is a factor of five less than Figure 3(b). The maximum in precipitation index *aP34* occurs during December of 2002, 2004 and 2006. Phase locking is elegantly confirmed by plotting the average monthly values of precipitation index *aP34* versus precipitation index *hP34* during the precipitation index *aP34*'*s* phase-locked cycle. One finds closed Lissajous loops where the number of loops is the subharmonic number for that phase-locked segment. Lissajous plots for segments 9 and 10 are shown in Figure 4(a) and b. Note that the y-axis in Figure 4(b) is a factor of five less than Figure 4(a). Both of the Lissajous loops for segment 10 are comparable in magnitude to the smallest loop for segment 9.

4.3. Discussion of results on precipitation index *P34*

The precipitation index *P34* (Figure 1(a)) contains both a high frequency component *hP34* (Figure 2(a)) and a low frequency component *aP34* (Figure 1(b)). Both are necessary to obtain a complete appreciation of the underlying phenomena.

Precipitation index *hP34* has an amplitude of about 2 mm day^{-1}. The autocorrelation function shows a sustained oscillation of 1.0 cycle year^{-1} whose amplitude is not decreasing, implying an external forcing. Since the oscillation frequency is 1.0 cycle year^{-1}, this 1.0 cycle year^{-1} oscillation almost certainly originates from the solar irradiance that has an annual component of amplitude of 11.3 W/m^2. DK1 called this annual component of the solar irradiance the 'Climate Pacemaker'. (Note. The 'Pacemaker' component of amplitude 11.3 W m^{-2} should not be confused with the seasonal component which is observed in high latitudes with amplitudes much larger.) The maximum occurs in early January when Earth is at perihelion. The average of the monthly values of precipitation index *hP34* has a maximum during April; one would expect this maximum to occur several months after perihelion because of the high specific heat capacity of the oceans. See also Douglass and Knox (2009).

Precipitation index *aP34* shows four phase-locked time segments since 1979. For example, from 1990 to 2000 precipitation index *aP34* shows phase locking to the annual term at the third subharmonic (period 3 years). The maxima occur during November of 1991, 1994 and 1997.

4.4. Comparison of precipitation index *P34* and sea surface temperature index SST3.4

Delayed correlation plots of precipitation index *aP34* versus sea surface temperature index *aSST3.4* were made for each of the four phase-locked segments (not shown). The value of the delay is that delay which gave the largest coefficient of determination R^2. The regression coefficients were positive and ranged from 0.66 to 2.09 °C (mm/day)$^{-1}$; precipitation index *aP34* lagged from 0 to 3 months, indicating the non-stationarity of the precipitation–temperature relationship (Table 1). The parameters changed abruptly from one segment to the next. Note that the values from the regression analysis depend weakly on the ends of the segments.

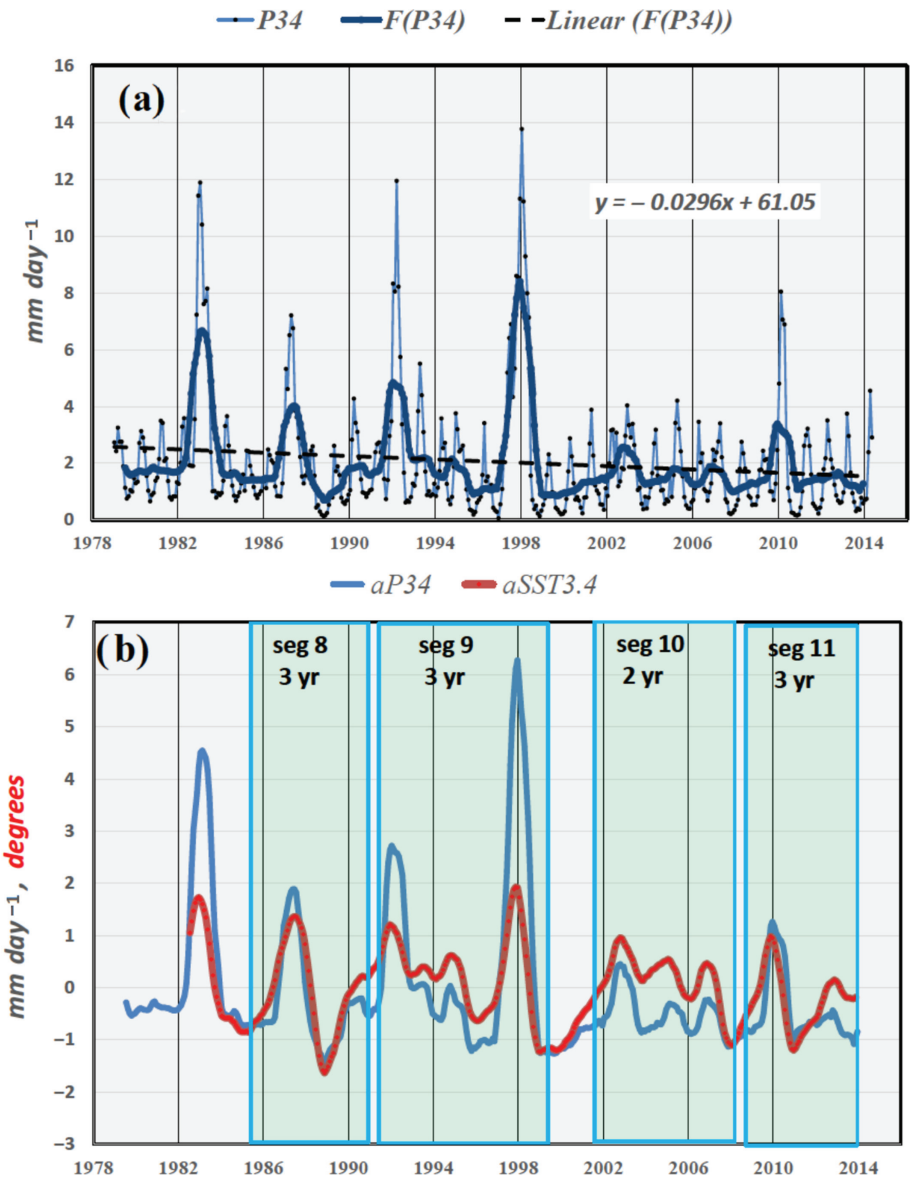

Figure 1. Low frequency (<1.0 cycles/year) indices. (a) Precipitation index *P34* (thin) and filtered precipitation index ***F****(P34)* (thick). (b) Precipitation index *aP34* and sea surface temperature index *aSST3.4*. (c) The 4 phase-locked time segments are indicated by shaded rectangles.

Table 1. Phase-locked states of *aSST3.4* from Douglass (2011) and *aP34* (this article).

Segment	Date range	Period and correlation
Seg8		3 years
aSST3.4	September 1985–December 1990	*aP34 = 1.06*aSST3.4*
aP34	October 1985–January 1989	$R^2 = 0.86$, delay of *aP34* = 0 months
Seg 9		3 years
aSST3.4	June 1991–January 1999	*aP34 = 0.66*aSST3.4*
aP34	January 1991–November 1999	$R^2 = 0.71$, delay of *aP34* = 2 months
Seg 10		2 years
aSST3.4	January 2001–March 2008	*aP34 = 1.06*aSST3.4*
aP34	August 2001–July 2008	$R^2 = 0.86$, delay of *aP34* = 1 months
Seg 11		3 years
aSST3.4	March 2008–end (2011)	*aP34 = 1.17*aSST3.4*
aP34	July 2008–end(December 2013)	$R^2 = 0.86$, delay of *aP34* = 3 months
Range	1979–2013	*hP34 = 1.74*hSST3.4* $R^2 = 0.79$, delay of *hP34* = 2 months

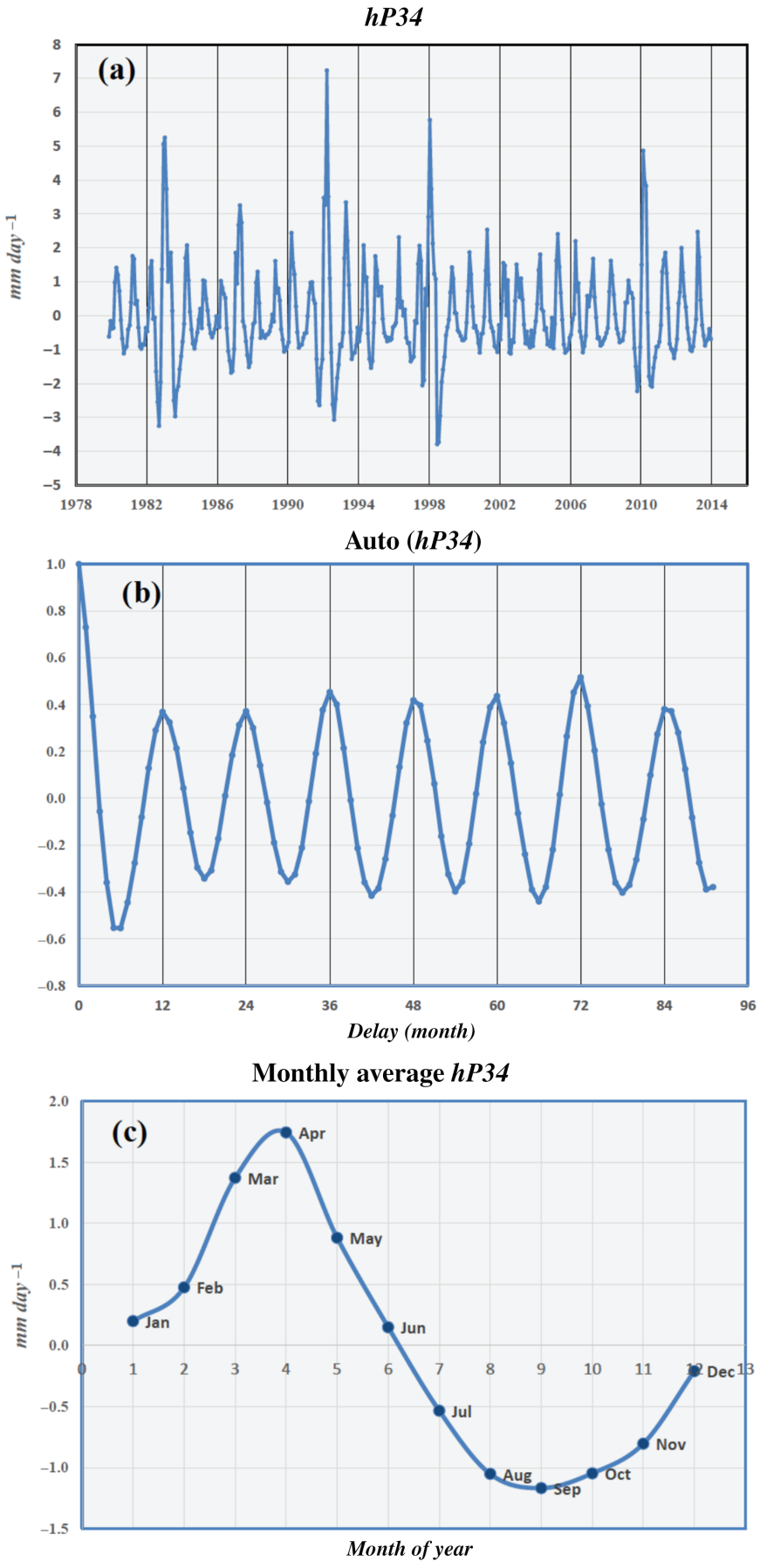

Figure 2. High frequency (≥1.0 cycles/year) precipitation index *hP34*. (a) Raw data. Note the annual cycle. (b) Autocorrelation function. Plot shows sustained oscillations at 1.0 cycles at large values of delay. (c) The average of each month of the cycle. Maximum occurs during April.

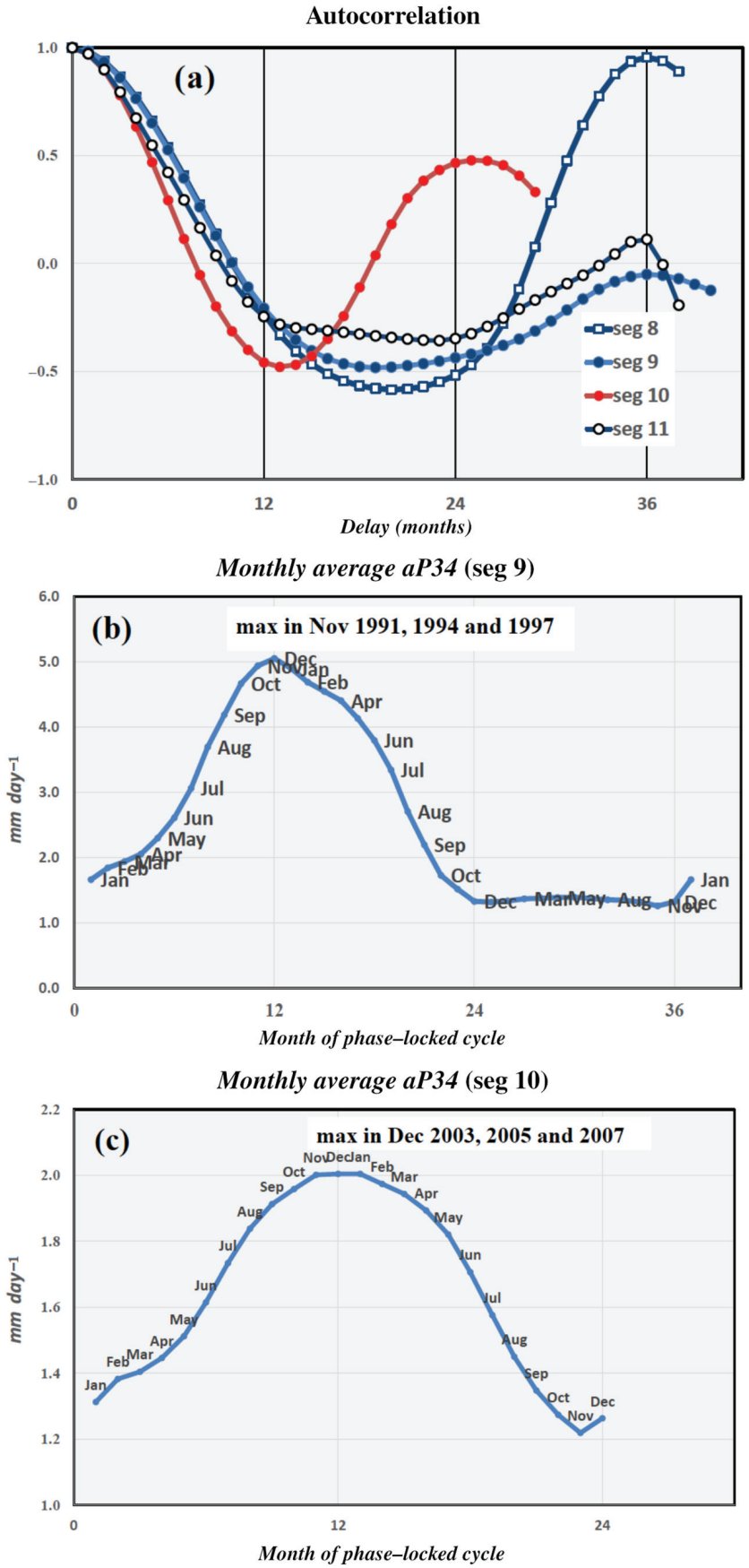

Figure 3. Plots related to the low frequency *aP34* precipitation index. (a) Autocorrelation of the four phase-locked segments (8, 9, 10, and 11) showing periodicities of 2- or 3-years. (b) Monthly average of phase-locked segment 9 (period 36 months). The maximum is the average of the values for November 1991, 1994, and 1997. (c) Monthly average of phase-locked segment 10 (period 24 months). The maximum is the average of the values for December 2003, 2005, and 2007.

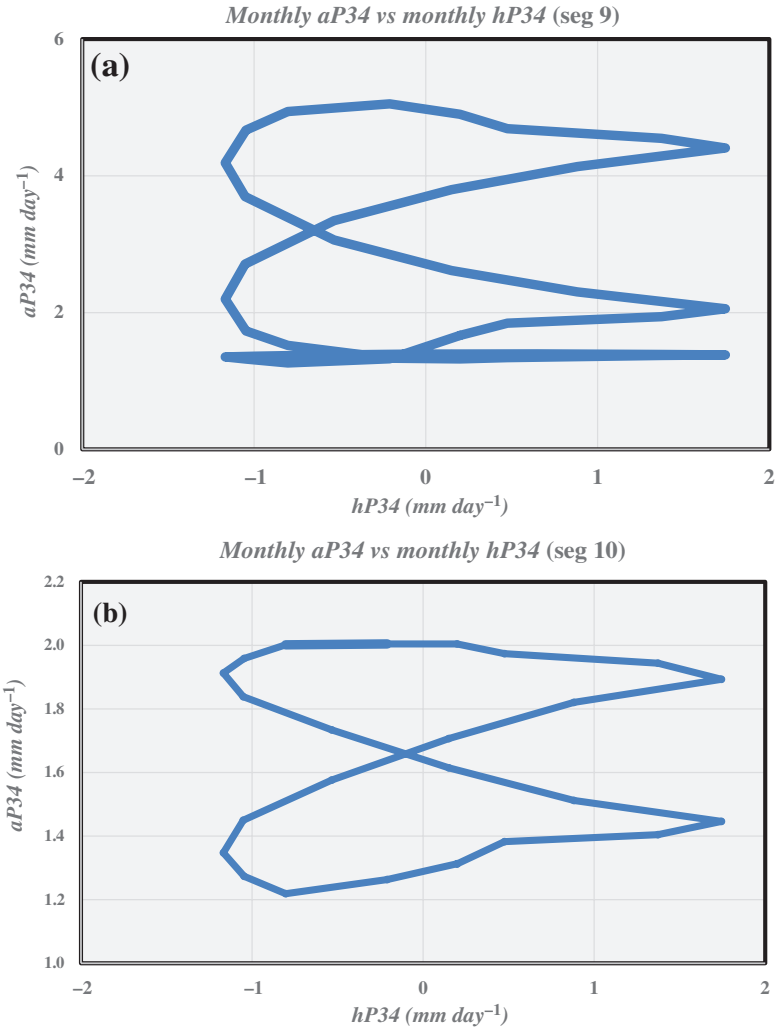

Figure 4. Lissajous plot of precipitation index *aP34* versus precipitation index *hP34*. Number of loops gives the subharminic number *n*. (a) Phase-locked segment 9. $n = 3$. (b) Phase-locked segment 10. n=2. (c).

One interesting finding was that the segment showing 2-year periodicity had the weakest precipitation response to temperature (lowest regression coefficient; see Table 1).

5. Discussion

5.1. Phase locking, nonlinearity and regression coefficient

In his report of 10 sequentially numbered phase-locked states of periods 2 and 3 years, Douglass (2011) pointed out that the phenomena of phase locking is well known in the field of nonlinear dynamics (Stoker, 1950). Stoker shows that for the example of a *1D* nonlinear oscillator of intrinsic frequency $\boldsymbol{\omega_0}$ driven by a forcing F at frequency $\boldsymbol{\omega_F}$ that there is a response at $\boldsymbol{\omega_F}$ which is out of phase with F. In addition, there can be a phase-locked response at the subharmonics of $\boldsymbol{\omega_F}$ (Note. This is not $\boldsymbol{\omega_0}$) if certain conditions of stability involving the nonlinear coupling are met–there is a region of stability in parameter space, which has upper and lower bounds. If the parameters change and take the system out of this region, the subharmonic behavior will abruptly cease. When the nonlinear terms are removed there are no subharmonic solutions. The phase-locking phenomena reported in this article are very similar to this case.

For the atmospheric/oceanic climate system, the existence of nonlinearities is inferred from the observation of phase-locked states. However, determination the nature of the nonlinear interactions in the climate system containing *P34* and *SST3.4* is beyond the scope of this study.

The explanation of the observed regression coefficient between precipitation index *aP34* and sea surface temperature index *aSST3.4* and the delay of precipitation index *aP34* is also left to a future study.

5.2. Prior studies

These results are consistent with the findings of Kumar and Hoerling (2003). They report that the peak in anomalous ocean surface warming of an El Niño event typically occurs in early winter (e.g. Figure 3(b) and

(c)), yet the climatological SSTs are not a maximum until Spring (see Figure 2(c)). The weaker deviations from the mean at this time of year more effectively excite the convective process that relies on energy availability, determined from absolute *SST*. Precipitation indices that take into account the change in the zonal gradient of rainfall, such as the ENSO Precipitation Index, mirror the Southern Oscillation and are concurrent with or can even lead *SST3.4* (see Figure 7 in Curtis and Adler, 2000). Further, it should be noted that ENSO has a large control on *SST* in the eastern Pacific. Compo and Sardeshmukh (2010) isolated the ENSO contribution to global *SST*, and after removing this signal found that the ENSO-unrelated component of the observed trend was towards cooling in the Region 3.4. Thus, reported trends in increasing rainfall in the eastern Pacific (e.g. Adler *et al.*, 2008) are more likely to be a reflection of ENSO rather than other natural or anthropogenic forcings (Compo and Sardeshmukh, 2010).

6. Conclusions

It is found that the precipitation data *P34* in Region 3.4 has four distinct time segments since 1979 that show the same subharmonic phase-locking phenomena at 2- and 3-year periods that has been reported in many other climate indices, such as sea surface temperature index *SST3.4*; atmospheric pressure variation in the western Pacific, *SOI*; temperature anomalies in the tropical troposphere, *TLT*; tropical easterly winds, *W3*; and the global ocean temperature.

It is asserted that the associated climate system is driven by a forcing of solar origin that has two manifestations: (1) A direct phase-locked response to what is identified as a solar forcing at a frequency of 1.0 cycle year^{-1}; (2) A phase-locked response at either the second or third subharmonic of the putative solar forcing. Observation of subharmonics implies the existence of a nonlinear interaction that is not identified. However, if one could determine the energy of each state, one might find that the difference is small and that the fluctuations determine which state is chosen.

The climate system is presently (May 2015) in a phase-locked state of periodicity 3 years. This state, which began in 2008, contains a maximum (El Niño) at about 2010 followed by a minimum (La Niña) followed by a maximum (weak El Niño at about 2013). If the climate system remains in this phase-locked state, the next maximum will not occur until about November 2015–January 2016.

In addition, the correlation between precipitation index *P34* and the commonly used El Nino/La Nina index *SST3.4* was determined for the phase-locked segments. The regression coefficient k (*P34* = *k*SST3.4*) was different for each phase-locked segment, with the smallest k being related to the 2-year segment.

Acknowledgements

The authors would like to acknowledge Dr. G. J. Huffman, Dr. G. Gu, Dr. R. Nieto-Ferreira, and Dr. R. S. Knox for helpful discussions which improved earlier versions of this manuscript.

References

Adler RF, Huffman GJ, Chang A, Ferraro R, Xie P, Janowiak J, Rudolf B, Schneider U, Curtis S, Bolvin D, Gruber A, Susskind J, Arkin P. 2003. The version 2 Global Precipitation Climatology Project (GPCP) monthly precipitation analysis (1979–present). *Journal of Hydrometeorology* **4**: 1147–1167.

Adler RF, Gu G, Wang J-J, Huffman GJ, Curtis S, Bolvin D. 2008. Relationships between global precipitation and surface temperature on inter-annual and longer time scales (1979–2006). *Journal of Geophysical Research-Atmospheres* **113**: D22104, doi: 10.1029/2008JD010536.

Allan RP, Soden BJ, John VO, Ingram W, Good P. 2010. Current changes in tropical precipitation. *Environmental Research Letters* **5**: 025205, doi: 10.1088/1748-9326/5/2/025205.

Bratcher AJ, Giese BS. 2002. Tropical Pacific decadal variability and global warming. *Geophysical Research Letters* **29**: 1918, doi: 10.1029/2002GL015191.

Compo GP, Sardeshmukh PD. 2010. Removing ENSO related variations from the climate record. *Journal of Climate* **23**: 1957–1978.

Curtis S, Adler RF. 2000. ENSO indices based upon patterns of satellite-derived precipitation. *Journal of Climate* **13**: 2736–2793.

Douglass DH. 2010. Topology of Earth's climate indices and phase-locked states. *Physics Letters A* **374**: 4164–4168.

Douglass DH. 2011. The Pacific sea surface temperature. *Physics Letters A* **376**: 128–135.

Douglass DH. 2013. Phase-locked states and abrupt climate shifts in Pacific climate indices. *Physics Letters A* **377**: 1749–1755.

Douglass DH, Knox RS. 2009. Ocean heat content and Earth's radiation imbalance. *Physics Letters A* **373**: 3296–3300.

Douglass DH, Knox RS. 2015a. The sun is the climate pacemaker I. Equatorial Pacific Ocean temperatures. *Physics Letters A* **379**: 823–829.

Douglass DH, Knox RS. 2015b. The sun is the climate pacemaker II. Global ocean temperatures. *Physics Letters A* **379**: 830–834.

Ebbesmeyer CC, Cayan DR, McLain DR, Nichols FH, Peterson DH, Redmond KT. 1991. 1976 step in the Pacific climate: Forty environmental changes between 1968–1975 and 1977–1984. In *Proceedings of the 7th Annual Pacific Climate Workshop*, *April 1990*, Interagency Ecological Study Program. Report 26, Betancourt JL, Tharp VL (eds.). California Department of Water Resources; 115–126.

Gu G, Adler RF. 2011. Precipitation and temperature variations on the interannual time scale: assessing the impact of ENSO and volcanic eruptions. *Journal of Climate* **24**: 2258–2270.

Huffman GJ, Adler RF, Bolvin DT, Gu G. 2009. Improving the global precipitation record: GPCP Version 2.1. *Geophysical Research Letters* **36**: L17808, doi: 10.1029/2009GL040000.

Kumar A, Hoerling MP. 2003. The nature and causes for the delayed atmospheric response to El Niño. *Journal of Climate* **16**: 1391–1403.

Liu C, Allan RP. 2012. Multisatellite observed responses of precipitation and extremes to interannual climate variability. *Journal of Geophysical Research* **117**: D03101, doi: 10.1029/2011JD016568.

NASA/GSFC. 2015. GPCP version 2.2. http://precip.gsfc.nasa.gov (accessed 8 June 2015).

NOAA/CPC. 2015. SST3.4 data. http://www.cpc.ncep.noaa.gov/data/indices/ (accessed 8 June 2015).

Stoker JJ. 1950. *Nonlinear Vibrations*. Interscience Publishers: New York.

Trenberth K. 1990. Recent observed interdecadal climate changes in the northern hemisphere. *Bulletin of the American Meteorological Society* **71**: 988–993.

Weisstein EW. 2015. Lissajous Curve. *MathWorld*–A Wolfram Web Resource. http://mathworld.wolfram.com/LissajousCurve.html (accessed 8 June 2015).